Eng. & Tech. Journal, Vol. 29, No.9, 2011

Cutting Forces Prediction in Ball End Milling

Dr. Hussain S. Kitan*, Dr.Bahaa I. Kadhim & Dr. Susan A. Abdulrazzaq***

Received on: 24/1/2010
Accepted on: 7/4/2011

Abstract

In curved surface machining, parametric surface representation is normally used for computer aided design (CAD). Parametric surfaces are often machined using a flat end mill for roughing and ball end mill for finishing.

The core of this work is to propose and implement a model that is able to estimate the cutting force in milling parametric surfaces with HSS ball end cutter of different diameters. For this purpose, a mechanistic model has been developed to calculate the cutting forces by dividing the cutting edge into small discrete elements and applying simple mathematical expressions for the cutting force estimation, once the force of each discrete element is calculated, these elements summed up along the cutting edge to obtain the resulting cutting force. The slope (inclination angle α) of the surface was included to the model to estimate the influence of different conditions of the slope ($-90^o \langle \alpha \langle +90^o$) which most parametric surfaces included. The results showed that the predicted results deviate from experimental by (0.6-11 %) for Fx, by (2-10 %) for Fy and by (0.18-14 %) for Fz

Keywords: Cutting Forces, Ball end milling, parametric surface

تنبؤ قوى القطع لعمليات التفريز بالعدد الاصبعية ذات النهاية الكروية

الخلاصة

في تشغيل السطوح المنحنية , يعتمد المفهوم البارامتري كاساس للتمثيل الهندسي والتصميم المعان بالحاسوب (CAD), وتشغل السطوح البارامترية باستخدام عدة تفريز اصبعية ذات نهاية مستوية (Flat end mill) للتشغيل الخشن (التشغيل الاولي) , في حين تستخدم عدة تفريز اصبعية ذات نهاية كروية (Ball end mill) للتشغيل النهائي.

أن الهدف الاساس لهذا البحث هو اقتراح انموذج لحساب وتقدير قوى القطع في تفريز السطوح البارامترية المشغلة بعدد أصبعية ذات نهاية كروية من صلب السرعات العالي وباقطار مختلفة حيث اعتمد هذا الانموذج المفهوم التطبيقي في حساب قوى القطع وذلك بتقسيم الحد القاطع الى عدد معين من الشرائح وحساب قوى القطع لكل شريحة لوحدها وباعتماد دوال التحويل المناسبة ثم جمع القوى للعدد المحدد من الشرائح تمكنا من الحصول على قوى القطع الكلية.ادخل متغير مهم للانموذج وهو ميل السطح المشغل المتمثل بزاوية(α)وذلك لبيان تأثير الحالات المختلفة للميل(90›α›90-),والتي تشملها معظم السطوح البارامترية ,على قوى القطع.بينت النتائج تقارب بين الانموذج المقترح والمسجلة عمليا" من ناحيتي القيم والسلوك. وبمقارنة قيم القطع القصوى

*** Production Engineering and Metallurgy Department, University of Technology/ Baghdad**
****Engineering College of ALkawrzmi, University of Baghdad/Baghdad**

https://doi.org/10.30684/etj.29.9.12
2412-0758/University of Technology-Iraq, Baghdad, Iraq

سجلت الاختلافات الاتية :\
اختلاف قيم قوى القطع باتجاه محور (x) بقيم تتراوح بين 1-11 %
اختلاف قيم قوى القطع باتجاه محور (y) بقيم تتراوح بين 1-10 %
اختلاف قيم قوى القطع باتجاه محور (z) بقيم تتراوح بين 1-14 %

Introduction

Metal cutting mechanics can be analyzed by orthogonal and oblique models. However, nearly all practical cutting processes are oblique. Mechanics of oblique cutting has been investigated in several works, two important ones being by **Armarego** [1] and **Merchant** [2]. Although the formulation of the process mechanics in many of the studies is similar, there are significant differences in the approach used in implementing the models for force prediction of practical processes. The main difficulty in machining process modeling is obtaining the material data, and this is where the approaches vary from completely analytical to completely experimental.

One analytical approach is to use the flow stress and thermal properties of the work-piece material in the analysis. **Shatla, et al**. [3] divided ball-end mill into oblique cutting elements that have geometries and cutting conditions that vary with the location of the element on the cutting edge. Using flow stress relation and the thermal characteristics of Ti6Al4V alloy for each element, they predicted ball-end milling forces. Another analytical approach is so called, thermo-mechanical modeling. The material characteristics such as strain rate sensitivity, strain hardening and thermal softening are considered. This is the approach used by **Moufki, et al.** [4] where a thermo-mechanical model was employed for the oblique cutting process.

Yucesan, et al. [5] and **Lazoglu** [6] are among the authors who modeled 3-axis ball-end milling using the Model is based on the analytic representation of ball shaped helical flute geometry, and its rake and clearance surfaces. The pressure and friction coefficients are identified from a set of slot ball-end milling tests at different feeds and axial depth of cuts, and are used to predict the cutting forces for various cutting conditions. Lazoglu presented a mechanistic force model that has the ability to calculate the work-piece/cutter intersection domain automatically for a given cutter location (CL) file. An analytical approach was used to determine instantaneous chip load and cutting forces considering run-out. In the mechanics of milling approach, the cutting force coefficients are predicted using the oblique cutting model and the orthogonal cutting database.

Budak, et al. [7] presented the method for orthogonal to oblique transformation. Shear stress, shear angle and friction angle are identified from orthogonal turning tests and they are inserted into oblique cutting model for calculating cutting force coefficients. Edge force coefficients are directly taken from orthogonal cutting tests. Mechanics of milling approach was employed by several authors for cutting force prediction in 3-axis ball-end milling.

Yang, et al. [8], **Sadeghi** et al. [9] and **Tai,** et al**.** [10] are some of these authors. In their studies, engaged cutting edge is divided into differential oblique elements. Corresponding orthogonal database is transformed to these differential oblique elements and differential cutting forces are calculated. For each tool rotational position, the cutting forces are found by summing the differential cutting forces.

In one of the important works on ball-end milling, **Lee and Altintas** [11] modeled 3-axis ball-end milling using orthogonal to oblique transformation. They present a cutting force model based on establishment of a data base containing basic machining quantities evaluated from a set of standard orthogonal cutting tests. The most used models for the milling process modeling are semi-mechanistic. These kinds of models based their idea on dividing the cutting edge into small discrete elements as shown in fig. (1) And apply to each of these elements simple mathematical expressions for the cutting force estimation. The forces for each discrete element are calculated. They are summed up along the cutting edge obtaining in this way cutting force is resulted. The cutting edge discretization allows simplification of the cutting edge geometry as a sequence of linear segments [12].

Most of the models applied to ball-end mills are based on the same fundamental basis that is used for flat end-mills, with the slight difference on the tool geometry and the chip thickness calculation. However, these models only consider horizontal surface machining. In parametric surface machining positive and negative slopes in x- and y-directions can be found.

In this paper the calculation of the chip thickness is performed by an intersection of the cutting edge and the part. The work presented in this section is a model based on a mechanistic approach generalized for parametric surface machining. Therefore the work is based on mathematical formulation of chip thickness that is valid for any surface slope.

Cutting Forces Modelling

For each position of rotation of the ball-end mill, the proposal developed model is able to calculate the cutting forces. The cutting forces are calculated as oblique machining forces. To develop the mechanistic model, the following assumptions were used:

- The run-out effect is ignored since the rigid system is used.
- There is no built-up edge formation on the cutter.
- Wear occurs at high cutting speeds and will become negligible.

The Proposed Model

The developed proposed model calculates the cutting forces in three different following steps:

In the **first step** the position of the ball-end mill cutting edges are calculated by cutting edge discretization.

Within the **second step**, by performing a coordinate transformation the chip thickness for the case of sloped surfaces is calculated.

Finally, in the **third step**, the cutting force result is estimated by numeric integration.

The cutting forces of a sharp tool can be given by the following expression[7]:

$$\begin{aligned} dF_t(\phi,k) &= K_{te}.dS + K_{tc}.t\ (\phi,k).db \\ dF_r(\phi,k) &= K_{re}.dS + K_{rc}.t\ (\phi,k).db \quad \cdots 1 \\ dF_a(\phi,k) &= K_{ae}.dS + K_{ac}.t\ (\phi,k).db \end{aligned}$$

where dFt, dFr, dFa (N) are the tangential, radial and axial components Fig.(2), Ktc, Krc, Kac: (N/mm2) are the shear specific coefficients, Kte, Kre, Kae (N/mm) are the edge specific coefficients, appendix ,**dS** (mm) is the length of each discrete elements of the cutting edge, **t** (mm) is the un-deformed chip thickness, and **db** (mm) is the chip width in each cutting edge discrete element.

As can be observed in Eq. (1), it is necessary to calculate the un-deformed chip thickness and the length of each discrete element of the cutting edge in order to apply the model. The calculation of these parameters requires a geometrical modelling of the tool. Once the cutting edge of the tool is positioned, a coordinate transformation is introduced in order to introduce the case of slope milling. Thus, the force over the cutting edge discrete elements is obtained and finally the resulting force is determined by a numerical integration.

Un-deformed Chip Thickness Formulation:

The instantaneous chip thickness in flat end milling operation can be obtained from [13]:

$$t_c = f_z.\sin(\phi) \ldots\ldots\ldots\ldots\ldots 2$$

Where tc is the instantaneous chip thickness, f_z is the feed per tooth and Ø is the radial immersion angle of cutting point. In machining parametric surfaces the formulation for ball end mill should be modified, since the chip thickness varies along the cutting edge as the depth of cut is changed. The chip thickness in eq.(2) combines only rotational and linear straight motion, while in machining parametric surfaces, rotational motion , and non-horizontal cutter feed motion and spherical part of the ball-end mill should be combined for an accurate chip thickness. In ball-end milling the eq. (2) have been modified by introducing the effect of axial immersion angle (k) of the spherical part of the tool on the un-deformed chip thickness [14], [15],

$$t_c = f_z.\sin\phi.\sin k \ldots\ldots\ldots 3$$

The non-horizontal cutter feed motion for ball end milling process with a horizontal feed component (f_h) and vertical feed component (f_v) results are shown for different cases in Fig. (3)When the cutter moves upwards or downwards with feed inclination angle, the feed direction vector is not perpendicular to the cutter rotation vector, and the cutting element produce different un-deformed chip geometry, as shown in fig.(4), in machining parametric surfaces positive and negative angles (α) are found due to surface inclination and this effect have been invested in this work to propose an equation to calculate un-deformed chip thickness.

The instantaneous un-deformed chip thickness for ball end mill cutter in machining parametric surfaces that consist different inclination angles is proposed as:

$$t_{new} = f_z.\sin(\phi).\sin(k).\cos(\alpha) \ldots 4$$

Where (*t new*) is the instantaneous chip thickness, f_z is the feed per tooth, Ø is the radial immersion angle of the cutting point, *k* is axial immersion angle, and α is the surface inclination angle ($-90^o \langle \alpha \langle 90^o$) Fig. (3).

Mechanistic Cutting Force Model

The uncut chip thickness $t(\phi_j, k)$ is measured normal to the cutting edge, and varies along the cutting edge as represented in eq.(4)

As shown in Fig. (4)

$$db = dz / \sin k \ldots\ldots\ldots 5$$

Substitute eq. (5) in eq. (4) yields:

$$t_{new} = f_z.\sin(\phi)..\cos(\alpha).dz/\text{db}...6$$

Substitute eq.(6) in eq. [1] yields:

$$\left.\begin{aligned} dF_{t,j}(\phi_j,k) &= K_{te}dS + K_{tc}\,f_z\sin\phi_j.\cos\alpha.dz \\ dF_{r,j}(\phi_j,k) &= K_{re}dS + K_{rc}\,f_z\sin\phi_j.\cos\alpha.dz \\ dF_{a,j}(\phi_j,k) &= K_{ae}dS + K_{ac}\,f_z\sin\phi_j.\cos\alpha.dz \end{aligned}\right] \quad .7$$

The tangential, radial, and axial forces are resolved in feed (X), normal (Y), and axial (Z) directions by the following transformation:

Two rotational transformation matrices have to be inserted to the set of equation (7) in order to make the tangential, radial and axial forces parallel to the global coordinate system (x,y,z). The first rotational matrix inserted to make the Ft-direction parallel to y-direction and this can be achieved by rotating the local coordinate system (i,j,k) around the z-axis by (90-Ø) clockwise as shown in Fig.(2)

$$\left.\begin{aligned} [T_1] &= \begin{bmatrix} \cos(90-\phi) & \sin(90-\phi) & 0 \\ -\sin(90-\phi) & \cos(90-\phi) & 0 \\ 0 & 0 & 1 \end{bmatrix} \\ [T_1] &= \begin{bmatrix} \sin\phi & \cos\phi & 0 \\ -\cos\phi & \sin\phi & 0 \\ 0 & 0 & 1 \end{bmatrix} \end{aligned}\right\} \quad ..8$$

The second rotational matrix is inserted to make the Fr-direction parallel to x-direction and Fa-direction parallel to z-axis. This can be achieved by rotating the local coordinate system (i,j,k) around the y-axis by (90-k) counter clockwise as shown in Fig.(2)

$$\left.\begin{aligned} [T_2] &= \begin{bmatrix} \cos(90-k) & 0 & -\sin(90-k) \\ 0 & 1 & 0 \\ \sin(90-k) & 0 & \cos(90-k) \end{bmatrix} \\ [T_2] &= \begin{bmatrix} \sin k & 0 & -\cos k \\ 0 & 1 & 0 \\ \cos k & 0 & \sin k \end{bmatrix} \end{aligned}\right\} \quad ..9$$

The composite transformation is achieved by multiplying the two matrices [T1 and T2]:

$$[T] = [T]_1[T_2]$$

$$T = \begin{bmatrix} \sin\phi & \cos\phi & 0 \\ -\cos\phi & \sin\phi & 0 \\ 0 & 0 & 1 \end{bmatrix}\begin{bmatrix} \sin k & 0 & -\cos k \\ 0 & 1 & 0 \\ \cos k & 0 & \sin k \end{bmatrix}$$

$$[T] = \begin{bmatrix} \sin k\sin\phi & \cos\phi & -\cos k\sin\phi \\ -\sin k\cos\phi & \sin\phi & \cos k\cos\phi \\ \cos k & 0 & \sin k \end{bmatrix} \ldots 10$$

$$\begin{bmatrix} dF_{x,j}(\phi_j,z) \\ dF_{y,j}(\phi_j,z) \\ dF_{z,j}(\phi_j,z) \end{bmatrix} = \begin{bmatrix} \sin k\sin\phi & \cos\phi & -\cos k\sin\phi \\ -\sin k\cos\phi & \sin\phi & \cos k\cos\phi \\ \cos k & 0 & \sin k \end{bmatrix} \times \begin{bmatrix} dF_{r,j}(\phi_j,z) \\ dF_{t,j}(\phi_j,z) \\ dF_{a,j}(\phi_j,z) \end{bmatrix} 11$$

By substituting eq. (7) in eq. (11) yields :

$$\begin{bmatrix} dF_{x,j}(\phi_j,z) \\ dF_{y,j}(\phi_j,z) \\ dF_{z,j}(\phi_j,z) \end{bmatrix} = \begin{bmatrix} \sin k\sin\phi & \cos\phi & -\cos k\sin\phi \\ -\sin k\cos\phi & \sin\phi & \cos k\cos\phi \\ \cos k & 0 & \sin k \end{bmatrix}\begin{bmatrix} K_{rc}\,f_z\sin\phi_j\cos\alpha.dz + K_{re}.ds \\ K_{tc}\,f_z\sin\phi_j\cos\alpha.dz + K_{te}.ds \\ K_{ac}\,f_z\sin\phi_j\cos\alpha.dz + K_{ae}.ds \end{bmatrix}$$

$$\begin{bmatrix} dF_{x,j}(\phi_j,z) \\ dF_{y,j}(\phi_j,z) \\ dF_{z,j}(\phi_j,z) \end{bmatrix} = f_z\cos\alpha\begin{bmatrix} K_{rc}\sin^2\phi_j\sin k & K_{tc}\sin\phi_j\cos\phi_j & -K_{ac}\sin^2\phi_j\cos k \\ -K_{rc}\sin\phi_j\cos\phi_j\sin k & K_{tc}\sin^2\phi_j & K_{ac}\sin\phi_j\cos\phi_j\cos k \\ K_{rc}\sin\phi_j\cos k & 0 & K_{ac}\sin\phi_j\sin k \end{bmatrix}\begin{bmatrix} dz \\ dz \\ dz \end{bmatrix} +$$

$$\begin{bmatrix} K_{re}\sin k\sin\phi_j & K_{te}\cos\phi_j & -K_{ae}\cos k\sin\phi_j \\ -K_{re}\sin k\cos\phi_j & K_{te}\sin\phi_j & K_{ae}\cos k\cos\phi_j \\ K_{re}\cos k & 0 & K_{ae}\sin k \end{bmatrix}\begin{bmatrix} ds \\ ds \\ ds \end{bmatrix} \ldots..12$$

Multiplying and dividing all the elements of the1st matrix in eq.(12) by (2) yields:

$$\begin{bmatrix} dF_{x,j}(\phi_j,z) \\ dF_{y,j}(\phi_j,z) \\ dF_{z,j}(\phi_j,z) \end{bmatrix} = \frac{f_z}{2}\cos\alpha\begin{bmatrix} 2K_{rc}\sin^2\phi_j\sin k & K_{tc}\sin 2\phi_j & -2K_{ac}\sin^2\phi_j\cos k \\ -K_{rc}\sin 2\phi_j\sin k & 2K_{tc}\sin^2\phi_j & K_{ac}\sin 2\phi_j\cos k \\ 2K_{rc}\sin\phi_j\cos k & 0 & 2K_{ac}\sin\phi_j\sin k \end{bmatrix}\begin{bmatrix} dz \\ dz \\ dz \end{bmatrix} +$$

$$\begin{bmatrix} K_{re}\sin k\sin\phi_j & K_{te}\cos\phi_j & -K_{ae}\cos k\sin\phi_j \\ -K_{re}\sin k\cos\phi_j & K_{te}\sin\phi_j & K_{ae}\cos k\cos\phi_j \\ K_{re}\cos k & 0 & K_{ae}\sin k \end{bmatrix}\begin{bmatrix} ds \\ ds \\ ds \end{bmatrix}.$$

13

Rearranging eq.(13)

$$\begin{bmatrix} dF_{x,j}(\phi_j,z) \\ dF_{y,j}(\phi_j,z) \\ dF_{z,j}(\phi_j,z) \end{bmatrix} = \frac{f_z}{2}\cos\alpha\begin{bmatrix} 2K_{rc}\sin^2\phi_j & K_{tc}\sin 2\phi_j & -2K_{ac}\sin^2\phi_j \\ -K_{rc}\sin 2\phi_j & 2K_{tc}\sin^2\phi_j & K_{ac}\sin 2\phi_j \\ 2K_{ac}\sin\phi_j & 0 & 2K_{rc}\sin\phi_j \end{bmatrix}\begin{bmatrix} \sin k\,dz \\ dz \\ \cos k\,dz \end{bmatrix} +$$

$$\begin{bmatrix} K_{re}\sin\phi_j & K_{te}\cos\phi_j & -K_{ae}\sin\phi_j \\ -K_{re}\cos\phi_j & K_{te}\sin\phi_j & K_{ae}\cos\phi_j \\ K_{ae} & 0 & K_{re} \end{bmatrix}\begin{bmatrix} \sin k\,ds \\ ds \\ \cos k\,ds \end{bmatrix} \ldots\ldots\ldots\ldots 14$$

The immersion angle Ø and slop angle α are independent of z and the integration boundaries z1 and z2 are independent of Ø and α, so they will be out side the integration while the instantaneous cutting forces at immersion angle Ø depend upon the axial immersion angle (k), and can be represented as in eq.(15), which is the proposed model of this work to calculate and simulate the cutting forces in machining parametric surfaces with ball end cutter.

$$\begin{bmatrix} dF_{x,j}(\phi_j, z) \\ dF_{y,j}(\phi_j, z) \\ dF_{z,j}(\phi_j, z) \end{bmatrix} = \frac{f_z}{2}\cos\alpha \begin{bmatrix} 2K_{rc}\sin^2\phi_j & K_{tc}\sin 2\phi_j & -2K_{ac}\sin^2\phi_j \\ -K_{rc}\sin 2\phi_j & 2K_{tc}\sin^2\phi_j & K_{ac}\sin 2\phi_j \\ 2K_{ac}\sin\phi_j & 0 & 2K_{rc}\sin\phi_j \end{bmatrix} \begin{bmatrix} A_1 \\ A_2 \\ A_3 \end{bmatrix} +$$

$$\begin{bmatrix} K_{re}\sin\phi_j & K_{te}\cos\phi_j & -K_{ae}\sin\phi_j \\ -K_{re}\cos\phi_j & K_{te}\sin\phi_j & K_{ae}\cos\phi_j \\ K_{ae} & 0 & K_{re} \end{bmatrix} \begin{bmatrix} B_1 \\ B_2 \\ B_3 \end{bmatrix} \quad .15$$

A and **B** represent the influence of cutter geometry on the average cutting and edge forces. They have to be evaluated as follows:

$$\left.\begin{aligned} A1 &= \int_{z1}^{z2} \sin k(z)dz \\ A2 &= \int_{z1}^{z2} dz \\ A3 &= \int_{z1}^{z2} \cos k(z)dz \end{aligned}\right] \quad \ldots\ldots\ldots\ldots\ldots\ldots\ldots\ldots\ldots 16$$

$$\left.\begin{aligned} B1 &= \int_{z11}^{z2} \sin k(z)dS(z) \\ B2 &= \int_{z1}^{z2} dS(z) \\ B3 &= \int_{z1}^{z2} \cos k(z)dS(z) \end{aligned}\right] \quad \ldots\ldots\ldots\ldots\ldots\ldots\ldots\ldots 17$$

Experimental work

A large number of cutting tests were performed without lubrication on a vertical 3-axis CNC milling machine. The cutting tests were conducted on a CK45 carbon steel of the following chemical composition:

C: 0.45 Si: 0.21 Mn: 0.6 Cr: 0.1 Ni: 0.22 Cu: 0.2

While the dimension of the primary block is fixed for the three parametric surfaces which:

150 mm X 150 mm X100 mm

A kistler three components dynamometer model [9257B] has been used to measure the cutting forces, the output signals were recorded and stocked on a PC through a height-channel kistler charge amplifier.

A two fluted uncoated HSS [W6Mo5Cr4V2Al] ball-end mill Fig.(5)of the following chemical composition

C	W	Mo	C	V	Si	Mn	S	P	Al
1.20	6.75	5.50	4.2	2.20	0.3	0.25	0.2	0.022	0.80

With young modulus of (558×10^3 N/mm^2) with different diameters [Ø10mm, Ø12mm and Ø14mm] with a nominal helix angle of 30° and a nominal rake angle of 0° on a ball part were used in the experiments

Three different complex parametric surfaces Fig.(6) have been designed and implemented during this work, iso-parametric tool path generation technique were suggested and created by specifying the number of lines desired across the surface, and the parameter direction in which to travel (***t*** or ***s***) to perform the machining of all the three parametric surfaces

The output tool path for the three desired parametric surfaces from MATLAB as m.file has been linked with *UG-NX5* software to simulate ,generate G&M codes for part programming, and machined theseparametric surfaces using 3-axis CNC vertical milling machine.

The generated tool path by UG-NX translated to CIMCOEdit software to facilitate the operation of translation of information from UG-NX to the postprocessor of the CNC milling machine through the standard port RS232.

UG-NX software compatible to generate the tool path for 3-axis, 4-axis, and 5-axis CNC machines the window of UG-NX5 while managing 1st parametric surface is illustrated in Fig. (7).

Iso-parametric tool path have been used in this work, surface points are calculated as a function of (t, *s*) parameter space, the tool path indexed along the surface by incrementing (*t*) and (*s*). Tool path planning is accomplished by holding the (*s*) parameter constant and indexing the (*t*) parameter, which is *forward step.* The forward step increment (Δt) must be carefully chosen since tool movements are linearly interpolated and the chordal deviation between the straight lines and the actual surface must be less than the desired tolerance (δ). Side-step increment in (*s*) parameter (*side step g*) must be small enough to keep the scallop height between spherically shaped cutter paths to less than the desired tolerance.

The measured (from dynamometer) and predicted (from the proposed model) cutting forces in X, Y and Z-directions for different tool paths of the 1st parametric surface are compared and illustrates in table (2)

The measured (from dynamometer) and predicted (from the proposed model) cutting forces in X, Y and Z-directions for different inclined angles of 2nd parametric surface are compared and illustrates in table (3)

The measured (from dynamometer) and predicted (from the proposed model) cutting forces in X, Y and Z-directions for different inclined angles of 3rd parametric surface are compared and illustrates in table (4)

By comparing the results obtained by simulation with those of the experiments, the following results were established:

- The value from the mechanistic model coincide well with the values of experiments
- The process of change of the cutting forces with respect to angle of rotation of the milling cutter and the amplitude correspond well.

Also, the maximum values of predicted cutting forces components were compared with the experimental values. Absolute error percentages on the maximum values of the cutting forces in the three orthogonal directions were determined.

The results showed that the predicted results deviate from experimental:

by 0.6-11 % for Fx
by 2-10 % for Fy
by 0.18-14 % for Fz

Discussion

On the basis of the obtained results, the operation of analytical model of cutting forces can be confirmed by the experimental results.

The global force amplitude is well predicted for Fx and Fy cutting force components, but a more important amplitude offset appears on Fz (up to 15%). It is mainly due to the fact that the material flow which occurs around the cutting edge, in particular, the cutting edge is supposed to be perfectly sharp. The material flow and associated shearing occurring at the clearance face lead to a ploughing force. The ploughing force level becomes very significant around the tool end when cutting velocity and un-deformed chip thickness tend to zero. These limit cutting conditions appear at the tool tip and the resultant ploughing force value is high in this region. The direction of this ploughing force is mainly normal to the tool envelope and at the tool tip; this direction is close to be the z-direction. That is why the force Fz is more affected by this phenomenon and the predicted Fz values are lower than the measured ones. Hence, the difference between measured and predicted forces is proportional to the existing ploughing force. The ploughing effect can be limited by using a controlled tool work-piece inclination in 5-axis machining. Finally, according to the fact that its influence occurs mainly on Fz force component, which is less important for tool deflection, tool vibration calculation and then for surface finish prediction. Hence, the ploughing force was not taken into consideration in this work.

Conclusions

A cutting force model using the mathematical formulation is suggested to calculate the cutting force when machining parametric surfaces. In this model, the cutting forces can be predicted precisely. Ball-end milling is modeled by using mechanistic approach of oblique cutting, applied for each active cutting edge element. The obtained results gave a good approximation for the cutting forces and the main experimental tendencies are retrieved. The modelling accuracy allows understanding of the cutting behaviour and to simulate cutting forces in order to enhance surface integrity, tool life, stability and productivity by optimizing cutting conditions, tool path, tool work-piece inclination and tool geometry.

Various cutting tests of inclined surfaces were performed. Comparing the measured cutting force with the simulated profiles for one tooth in various cutting modes, the calculated forces are in good agreement with the measured cutting forces. Because the tool moves along the left and right side of the previous tool path in machining 1st parametric surface, the size and location of the cutter contact area are not symmetric at 0° of surface inclination angle, so the measured cutting forces differ from the simulated ones as shown in the table (2).

To show validity of the model when the surface inclination angle varies, another two parametric surfaces were machined (2nd and 3rd surfaces). The surface inclination angle is zero at the peak of the 2nd parametric surface as it is positive during down-cut and negative during up-cut. The calculated forces and test results show good agreement as shown in the tables (3 and 4).As the absolute value of surface inclination angle increases, the cutter contact area moves outward and the size decreases. It is obvious that the size of the cutter contact area is significantly affected by the inclination angle of the surface.

The shape of the curves of measured and predicted cutting forces is similar and the amplitude slightly differs. The global force amplitude is well predicted for *Fx* and *Fy* cutting force components (offset between 1 and 10%), but a more important amplitude offset appears for the *Fz* component (1-14%). The amplitude offsets are mainly due to the repetitive entries of the cutting edges in the work-piece material which induce cutting instability.

Through a series of experiments in machining three parametric surfaces, it is shown that the calculated forces are in good agreement with the experimental results and the shape of the envelope of measured and predicted cutting forces are similar and the amplitude slightly differs

References

[1] Armergo E. J. A. and Brown R. H., "The Machining of Metal ", Prentice-Hall, 1969.

[2] Merchant M. Eugene, "Basic Mechanics of Metal Cutting Process", 1971

[3] M. Shatla, T. Altan, "Analytical modeling of drilling and ball end milling, Journal of Material Processes Technology, Vol.98, pp 125–133, 2000.

[4] A.Moufki, A. Devillez, D. Dudzinski, A. Molinari, "Thermo mechanical modeling of oblique cutting and experimental validation", Int. J. Mach.

ASME Journal of Manufacturing Science and Engineering , pp 216–224, 1996.

[8] Yang M, Park H. "The prediction of cutting force in ball end milling".Int J.Machine Tools Manufacturing, Vol.31, pp 45–51, 1991.

[9] Sadeghi M. H., Tools Manufacture, Vol.44, pp 971–989, 2004.

[5] G. Yu¨cesan, Y. Altintas, , "Prediction of ball end milling forces", ASME Journal of Engineering for Industry, , pp 95–103, 1996.

[6] I. Lazoglu, Sculpture surface machining: "A generalized model of

ball-end milling force system", International Journal of Machine Tools and Manufacture, Vol.43, pp 453–462. 2003.

[7] E. Budak, Y. Altintas, , E.J.A. Armarego, "Prediction of milling force coefficients from orthogonal cutting data", Haghighat H. and Elbestawi M. A.," A solid modeler based Ball end milling process simulation", International Journal of Advance Manufacturing Technology, pp775-785, 2003.

[10] Tai C., Fuh K., "The prediction of cutting forces in the ball-end milling process", Journal of Material Processing Technology, Vol.54, pp 286-301, 1995.

[11] P. Lee, Y. Altintas, " Prediction of ball end milling forces from orthogonal cutting data" , International Journal of Machine Tools and Manufacture, Vol.36, pp 1059-1072, 1996..

[12] A.Lamikiz, L. N. Lopez, J. A. Sanchez and M. Selgado, " Cutting force estimation in sculptyred surface milling ", International Journal of Machine Tools & Manufacture, Vol.44, pp 1511-1526, 2004.

[13] H. Erdim, I. Lazoglu and B. Ozturk, " Feed rate scheduling strategies for free form surfaces ", International Journal of Machine Tools & Manufacture, Vol.46, pp 747-757, 2006.

[14] R.Salami, M. H. Sadeghi and B. Motakef, "Feed rate optimization for 3-axis ball end milling of sculptured surfaces ", International Journal of Machine Tools & Manufacture, Vol.47, pp 760-767, 2007.

[15]B. U. Guzel, I. Lazoglu, " Increasing productivity in sculptured surface machining via off-line piecewise variable feed rate scheduling based on the force system model" , International Journal of Machine Tools & Manufacture, Vol.44, pp 21-28, 2004.

Table (1) Characteristics of the CNC milling m/c used in the experimental work

Main Features of CNC Milling Machine	
Types of controller	HEIDENHAIN TNC430M
Method of the connection	USB cable, RS 232 cable, wireless
Maximum distance of travel	X-axis 710mm Y-axis 550 mm Z-axis 500mm
Max work piece weight	600 kg
Spindle power	5.5 to 7.5 kw
Spindle speed	100 to 18000 rpm
Rapid feed	30m/min
Cutter library	30 cutters
Time of cutter change	5 sec.

Table (2) Measured and predicted cutting forces of the 1st parametric surface

1st Parametric Surface HSS Ball-end mill ; CK45 Work-piece material Tool Dia. Ø10mm; Feed per tooth fz =0.10mm Forward step=1.85185 mm; Axial depth of cut =1 mm			
Inclination Angle (Deg)	Max Fx Measured (N)	Max Fx Predicted (N)	Error %
$\alpha = 0$, 41st Path	375.8917	360.109	4.2
$\alpha = 0$, 42nd Path	380.7245	360.109	5.4
$\alpha = 0$, 45th Path	375.977	360.109	4.2
$\alpha = 0$, 46th Path	352.755	360.109	2.1

Inclination Angle (Deg)	Max Fy Measured (N)	Max Fy Predicted (N)	Error %
$\alpha = 0$, 41st Path	270.6582	254.934	5.8
$\alpha = 0$, 42nd Path	271.184 negative direction	254.934 negative direction	6
$\alpha = 0$, 45th Path	241.211	254.934	5.7
$\alpha = 0$, 46th Path	261.993 negative direction	254.934 negative direction	2.7
Inclination Angle (Deg)	Max Fz Measured (N)	Max Fz Predicted (N)	Error %
$\alpha = 0$, 41st Path	256.9419	230.487	10.2
$\alpha = 0$, 42nd Path	253.1256	230.487	8.9
$\alpha = 0$, 45th Path	247.07	230.487	6.7
$\alpha = 0$, 46th Path	207.0311	230.487	11.3

Table (3) Measured and predicted cutting forces with various surface inclination angles (selected) in machining 2nd parametric surface.

2nd Parametric Surface HSS Ball-end mill ; CK45 Work-piece material Tool Dia. Ø12mm; Feed per tooth fz =0.12mm Forward step=1.9231 mm; Axial depth of cut =1 mm			
Inclination Angle (Deg)	Max Fx Measured (N)	Max Fx Predicted (N)	Error %
25.41	365.748	385.961	5.5
20.57	386.466	399.465	3.4
15.43	395.055	407.71	3.2
10.83	405.274	418.258	3.2
5.26	474.235	423.818	10.6

Inclination Angle (Deg)	Max Fy Measured (N)	Max Fy Predicted (N)	Error %
25.41	237.132	244.436	3.1
20.57	240.419	253.364	5.4
15.43	245.437	258.814	5.5
10.83	251.983	265.787	5.5
5.26	297.069	269.463	9.3
Inclination Angle (Deg)	Max Fz Measured (N)	Max Fz Predicted (N)	Error %
25.41	215.606	238.864	10.8
20.57	225.227	247.476	9.9
15.43	231.526	252.733	9.2
10.83	258.985	259.459	0.18
	240.196	263.004	9.5

Table (4) Measured and predicted cutting forces with various surface inclination angles (selected) in machining 3rd parametric surface.

3rd Parametric Surface HSS Ball-end mill ; CK45 Work-piece material Tool Dia. Ø14mm; Feed per tooth fz =0.14mm Radial depth of cut =2.1428 mm; Axial depth of cut = 1 mm

Inclination Angle (Deg)	Max Fx Measured (N)	Max Fx Predicted (N)	Error %
15.585	447.602	471.453	5.3
14.570	497.217	473.621	4.7
12.651	457.869	477.343	4.3
10.315	478.223	481.179	0.62
8.101	506.25	484.097	4.4

Inclination Angle (Deg)	Max Fy Measured (N)	Max Fy Predicted (N)	Error %
15.585	261.193	278.157	6.5
14.570	288.086	279.484	3
12.651	264.581	281.763	6.5
10.315	267.102	284.112	6.4
8.101	268.105	285.898	6.6
Inclination Angle (Deg)	**Max Fz Measured (N)**	**Max Fy Predicted (N)**	**Error %**
15.585	263.965	287.085	8.7
14.570	265.128	288.437	8.8
12.651	268.570	290.759	8.3
10.315	267.531	293.152	9.6
8.101	307.051	294.972	4.5

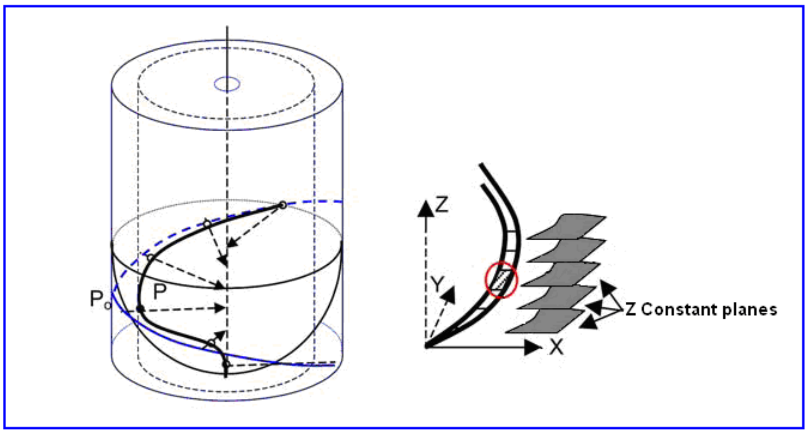

Figure (1) Cutting edge discretization [12]

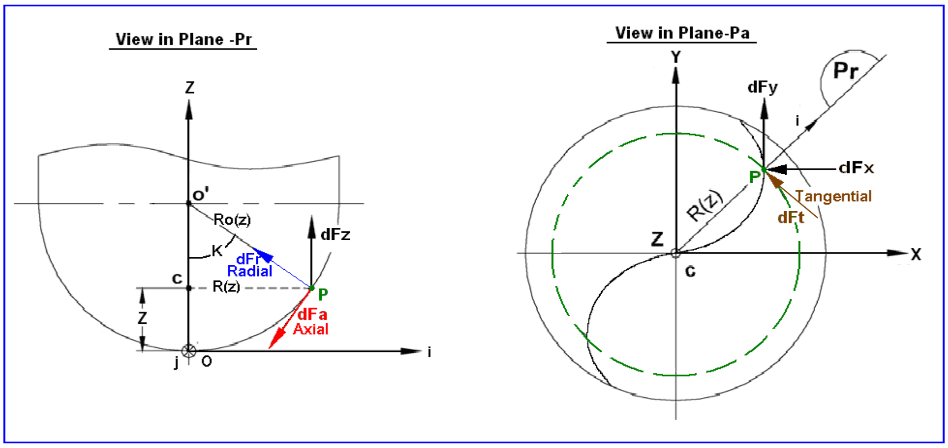

Figure (2) Elemental Cutting Forces

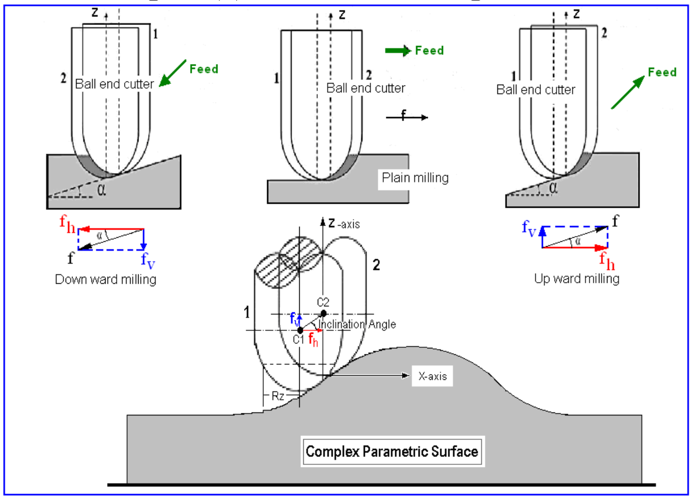

Figure (3) downward Milling, Upward Milling and Plain Milling cases in Machining Parametric surface

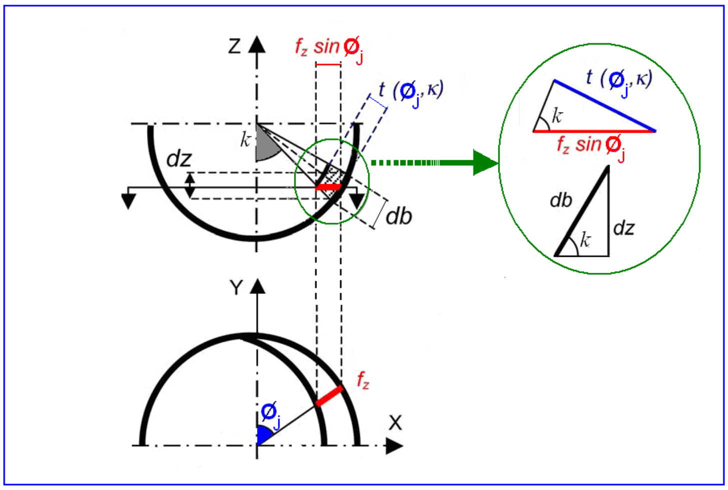

Figure (4) Un-cut chip thickness

Figure (5) Three Different Parametric Surfaces

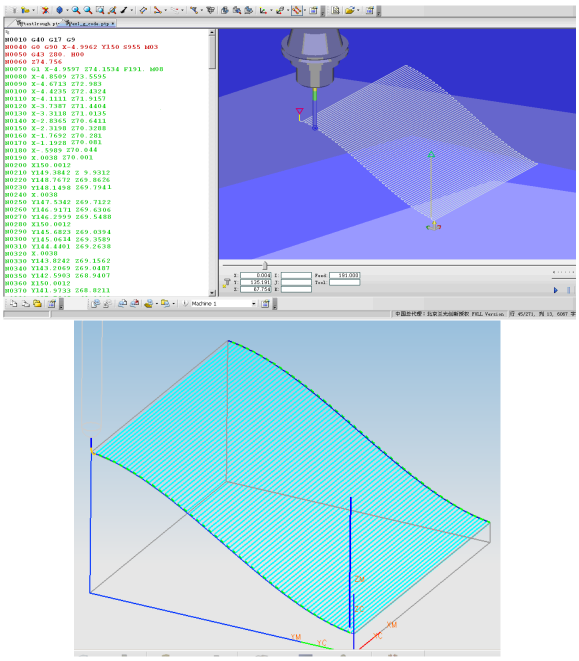

Figure (6) *UG-NX5* Main window while managing 1st parametric surface

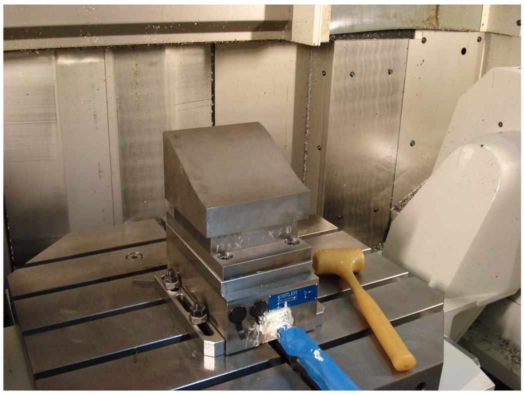

Figure (7) The finished Machined Parametric Surface No.1

Figure (8) The finished Machined Parametric Surface No.2

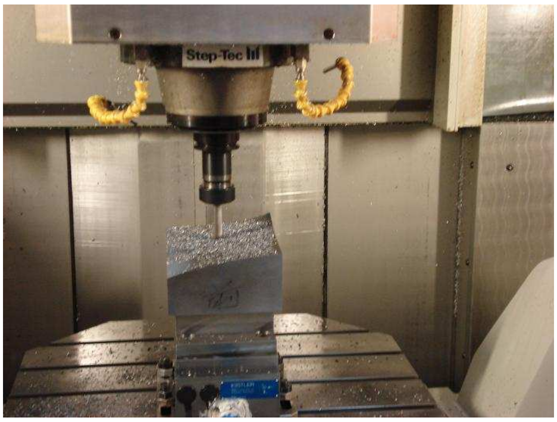

Figure (9) The finished Machined Parametric Surface No.3